

Composition of continental crust altered by the emergence of land plants

Christopher J. Spencer^{1*}, Neil S. Davies², Thomas M. Gernon³, Xi Wang¹, William J. McMahon², Taylor Rae I. Morrell¹, Thea Hincks³, Peir K. Pufahl¹, Alexander Brasier⁴, Marina Seraine¹, Gui-Mei Lu^{1,5}

*Corresponding author. Email: c.spencer@queensu.ca

¹Department of Geological Sciences and Geological Engineering, Queen's University; Kingston K7L 2N8, Ontario, Canada

²Department of Earth Sciences, University of Cambridge; Downing Street, Cambridge CB2 3EQ, United Kingdom

³School of Ocean & Earth Science, University of Southampton; Southampton SO14 3ZH, United Kingdom

⁴School of Geosciences, University of Aberdeen, King's College; Aberdeen AB24 3UE, United Kingdom

⁵State Key Laboratory of Geological Processes and Mineral Resources, School of Earth Sciences, China University of Geosciences; Wuhan 430074, China

The evolution of land plants during the Palaeozoic Era transformed Earth's biosphere. Because the Earth's surface and interior are linked by tectonic processes, the linked evolution of the biosphere and sedimentary rocks should be recorded as a near-contemporary shift in the composition of the continental crust. To test this hypothesis, we assessed the isotopic signatures of zircon formed at subduction zones where marine sediments are transported into the mantle, thereby recording interactions between surface environments and the deep Earth. Using oxygen and lutetium-hafnium isotopes of magmatic zircon that respectively track surface weathering (time-independent) and radiogenic decay (time-dependent), we find a correlation in the composition of continental crust after 430 Myr ago, which is coeval with the onset of enhanced complexity and stability in sedimentary systems related to the evolution of vascular plants. The expansion of terrestrial vegetation brought channelled sand-bed and meandering rivers, muddy floodplains, and thicker soils, lengthening the duration of weathering before final marine deposition. Collectively, our results suggest that the evolution of vascular plants coupled the degree of weathering and timescales of sediment routing to depositional basins where they were subsequently subducted and melted. The late Palaeozoic isotopic shift of zircon indicates that the greening of the continents was recorded in the deep Earth.

35 Plants are the dominant kingdom of life on Earth, accounting for ≈ 450 gigatons of a total ≈ 550
36 Gt of extant living biomass ¹, and successfully colonizing $\sim 84\%$ surface area of the presently
37 subaerially exposed continental crust ². Yet Earth's status as a 'green planet' is geologically
38 recent, and other than some millimetre-thick microbial mats ³, terrestrial vegetation was absent
39 for approximately 90% of the planet's history. Recently reported palynological evidence
40 indicates that the first embryophytes (land plants) likely evolved from aquatic charophyte algae,
41 that had begun to adapt to terrestrial settings by at least the early Ordovician (c. 480 Myr ago) ^{4,5}.
42 The earliest empirical fossil evidence for vegetated continents comes from cryptospores that
43 appear recurrently in strata onwards from the Middle Ordovician (c. 467-470 Myr ago) ⁶,
44 attesting to relative evolutionary stasis in which early land plants were restricted to wet coastal
45 environments, and maintained diminutive, low diversity, simple forms for the first 30-40 Myr of
46 their history ^{7,8}. Eventually this primitive vegetation became outcompeted by vascular plants, and
47 both spores and plant megafossils attest to a major late Silurian-Early Devonian adaptive
48 radiation of land plants (diversification, morphological innovation and increasing size) that
49 initiated at the end of the Llandovery Epoch (c. 433 Myr ago) ⁹.

50 **Land Plants and Riverine Sediments**

51 Early Palaeozoic land plants had profound impacts on Earth surface processes and geological
52 products. Fossil evidence for the advent of land plants is coeval with a step increase in the
53 amount of mudrock deposited in continental settings ^{10,11}. Throughout the Precambrian,
54 terrigenous mudrocks were primarily the product of physical erosion with limited pedogenic clay
55 mineral formation ¹². However, geochemical data suggest that in the early Palaeozoic, the
56 primary locus of the global 'clay mineral factory' shifted from the oceans to the land ¹³ as early
57 land plants induced the inception of new pathways in (micro)biologically mediated weathering.
58 Fossil evidence supports this notion, as Silurian plants—and their bacterial and fungal

59 symbionts—formed early plant ground covers that would have intensified clay mineral
60 weathering¹⁴.

61 The Early Devonian evolution of advanced rooting systems with root axes and meristems¹⁵
62 would have caused a further increase to the volume of the critical zone for terrigenous
63 weathering, promoting a greater root surface area and amplified connectivity with the reactive
64 near-surface environment¹⁶. The increased volume of mud and clay on the continents was likely
65 also boosted by the disruption of seaward transport of fine sediments by the retentive influences
66 of land plants as obstacles and stabilizers^{10,11,17}, and possibly by the capacity of their organic
67 matter to heighten mud flocculation and deposition¹⁸.

68 Physical sedimentary processes and products on the continents were also influenced by the
69 evolutionary adaptations of plants. Advances such as the evolution of vascular plant roots,
70 around 411 Myr ago¹⁵, and the earliest trees at 390-388 Myr ago^{19,20}, bound channel margins
71 and increased complexity in river geomorphology at a variety of spatio-temporal scales¹⁰. A
72 prominent impact is seen in the rise in abundance of mud-rich fluvial deposits during the Silurian
73 and Devonian, distinguishing them from more ancient mud-poor alluvium and attesting to an
74 increase in meandering river planforms¹⁰. Although rapidly migrating sandy meandering
75 systems were almost certainly in existence before the evolution of land plants¹⁰, the Silurian and
76 Devonian ushered in the first abundant mesoscale, muddy meandering channels²¹, which would
77 have both fragmented and lengthened source-to-sink sediment conduits and maintained stable
78 floodplains as long-lived sediment staging areas. Incorporation of the plant organic matter into
79 floodplain sediments also affected carbon cycling, driving enhanced production of calcrete
80 (calcium carbonate) in terrestrial sediments from the Silurian onwards^{22,23}. It seems likely that
81 the development of plants with rhizospheres in the Siluro-Devonian will also have directly
82 enhanced chemical rock weathering²⁴: a hypothesis that demands checking of suitable proxies.

83 The oxygen isotopic composition of the continental crust is one such proxy ²⁵. From the bulk
84 Earth average $\delta^{18}\text{O}$ of $\sim 5.5\text{‰}$ (as compared to Vienna Standard Mean Ocean Water) ²⁶, isotopic
85 fractionation during low-temperature weathering and water-rock interaction led to elevated
86 whole-rock $\delta^{18}\text{O}$ values in siliciclastic sedimentary rocks. Even in sparsely vegetated
87 environments, the weathering of silicate material results in higher $\delta^{18}\text{O}$ in sediments and minimal
88 post-depositional isotope exchange with ground or surface waters ²⁷. Whilst high $\delta^{18}\text{O}$ ($> 15\text{‰}$)
89 were present throughout the Proterozoic Eon and exhibit a marked increase across the Archean–
90 Proterozoic transition ²⁸, the distribution of $\delta^{18}\text{O}$ and chemical index of alteration of non-
91 glaciogenic mudrocks does not dramatically change throughout the Phanerozoic (Supplementary
92 Figure 1) ²⁸.

93 Conversely, empirical geologic evidence shows that the volume of continental mudrock
94 preserved in the geologic record expanded dramatically during the early Palaeozoic ¹¹. Models
95 have also predicted that the advent of land plants increased silicate weathering rates by a factor 2
96 to 10 (ref. ²⁴) albeit in a transitory way ²⁹, and an increase in silicate weathering and increased
97 CO_2 fixation via photosynthesis led to substantive cooling during the late Ordovician ³⁰ and
98 Devonian ³¹. These lines of evidence suggest that associated signals could be found in under-
99 explored archives, including Earth's zircon $\delta^{18}\text{O}$ record.

100 **Sediment Recycling in Magmatic Systems**

101 Sedimentary deposition along continental margins and within ocean basins ultimately leads to a
102 global fraction of that material becoming incorporated into magmatic systems during subduction
103 ^{32,33}. The most common loci of such activity are subduction zones where sedimentary material is
104 either subducted into the asthenosphere ³⁴, or melted in the upper crust along the periphery of
105 rising plutons ³⁵. While other convergent margins also form sediment-derived magmas (e.g.,

106 continental orogens ³⁶ and back-arc basins ³⁷), given the length of global subduction zones, these
107 are likely the largest contributor of magma influenced by sedimentary material ³⁸.

108 The influence of sediment on magmatic systems is most commonly tracked through geologic
109 time using $\delta^{18}\text{O}$ and U-Pb geochronology of the mineral, zircon ³⁹. It is understood that any
110 igneous rocks with $\delta^{18}\text{O}$ values divergent from the average mantle (~5.5‰) must have been in
111 part or wholly derived from supracrustal material ³⁹ and that the presence of a sedimentary $\delta^{18}\text{O}$
112 signature in magmatic zircon can be traced from some of the oldest terrestrial zircon (~4.27 Gyr
113 ago) ^{40,41} to the youngest exposed granites (818.5±9.6 kyr ago) ⁴². Another powerful isotopic tool
114 in zircon is Lu-Hf, where the radioactive β -decay of ¹⁷⁶Lu to ¹⁷⁶Hf allows for comparison of the
115 Lu-Hf isotopic composition of zircon at formation with the chondrite uniform reservoir and
116 depleted mantle. ¹⁷⁶Lu/¹⁷⁷Hf is displayed as ϵHf that is normalized to the chondrite uniform
117 reservoir.⁴³

118 **Tracing Sedimentary Components in Zircon**

119 We developed a new compilation of U-Pb, Lu-Hf, and O isotopic data from detrital zircon ⁵ to
120 evaluate secular change in their correlations (Fig. 1). To assess the correlation of ϵHf and $\delta^{18}\text{O}$
121 over time, we use a rolling window to visualize changes in the slope, r^2 , Pearson's correlation,
122 and Spearman's Rank correlation (Figs. 1F, 2) ⁵. We find no statistically reliable correlation
123 between ϵHf and $\delta^{18}\text{O}$ prior to 450 Myr ago. After ~430 Myr ago, however, ϵHf and $\delta^{18}\text{O}$ show a
124 strong correlation as well as a statistically significant step change between 450-430 Myr ago
125 (Fig. 2; Extended Data Fig. 2) ⁵. Covariance in independent zircon O and Lu-Hf isotopic datasets
126 (analyses not from the same zircon grains) has previously been linked to deglaciation and
127 sediment subduction following the Cryogenian global glaciation ⁴⁴. In contrast, this study
128 evaluates the correlation of O and Lu-Hf isotopes in individual zircon thus providing a unique

129 view at the grain scale ⁵. In addition, we expand upon the work of ref. ¹¹ through the application
130 of a step change algorithm to the percentage of mudrocks in sedimentary successions, which
131 reveals a significant increase at 430 Myr ago (Fig. 3; Extended Data Fig. 3) in tandem with the
132 late Silurian adaptive radiation of land plants ⁹. Assessment of tectonic subdivisions using the
133 timing of supercontinent assembly confirms that none of the periods of substantial collisional
134 orogenesis yield a statistically significant correlation between zircon ϵHf and $\delta^{18}\text{O}$ (Extended
135 Data Fig. 4) meaning that supercontinent tectonics can be ruled out as the driver of this signal ⁵.

136 The U-Pb and Lu-Hf isotope systems track magmatism and crystallization at temperatures
137 $>700^\circ\text{C}$ and thus document geologic processes occurring deep in Earth's crust and recording the
138 chronology of magmatic processes (i.e., mantle extraction and zircon crystallization). While the
139 oxygen isotopic compositions of zircon are also imparted within the magmatic system at depth,
140 elevated $\delta^{18}\text{O}$ indicates the melting of material that was once exposed at Earth's surface (i.e.,
141 (meta)sedimentary material; Fig. 1A). Given that the melting of (meta)sedimentary material
142 occurs in a multitude of magmatic rocks with sediments of varying ages ⁴⁵ and different tectonic
143 settings (e.g., young sediments in oceanic arcs; ³²; old sediments in collisional orogens; ³⁶), there
144 is no prima facie expectation for Lu-Hf and O isotopes in zircon to be correlated.

145 The post-430 Myr ago correlation between these two magmatic proxies implies some secular
146 change in the rates of sediment transport from source-to-sink, with the sediment sink
147 subsequently facilitating melting of sedimentary material. Importantly, the $\epsilon\text{Hf} - \delta^{18}\text{O}$ correlation
148 requires a diversity of processes including the formation of zircon with mantle-derived isotopic
149 signatures (both in Lu-Hf and O isotopes) along with the melting of progressively older and
150 more highly weathered sedimentary rocks. As mantle-derived magmatism forms the endmember
151 from which all primary crustal magmas form, the secular change discussed herein is assumed to
152 primarily represent sedimentary processes.

153 Due to the time-integrated nature of ϵHf , the comparison of ϵHf and $\delta^{18}\text{O}$ through time is
154 problematic. However, when dealing with narrow windows of time (<250 Myr) the amount of
155 radiogenic decay in the chondrite uniform reservoir (CHUR) is minimized. An alternative
156 assessment can be done by using crustal residence ages (depleted mantle model age minus
157 crystallization age). This however comes with an assumption of the $^{176}\text{Lu}/^{177}\text{Hf}$ applied globally.
158 Nevertheless, ϵHf versus $\delta^{18}\text{O}$ show broadly the same patterns as crustal residence versus $\delta^{18}\text{O}$
159 (Extended Data Fig. 5, Extended Data Fig. 6). We compare secular change of zircon
160 compositions with sedimentological and paleontological data to quantitatively understand
161 potential linkages between terrestrial biosphere evolution—including the expansion of vascular
162 land plants and their influence on source-to-sink sediment transfer—to the melting of sediments
163 in convergent margins and the composition of magmatic zircon and by proxy the continental
164 crust.

165 The widespread development of post-Archean continental freeboard ^{46,47} and the concomitant
166 increase in continental weathering is inferred from an increase of mudrock $\delta^{18}\text{O}$ throughout the
167 Proterozoic ²⁸; no equivalent secular change is apparent in post-Proterozoic mudrocks (Extended
168 Data Fig. 1). Therefore, the importance of progressive weathering and mudrock formation (and
169 thus facilitation of the increase in zircon $\delta^{18}\text{O}$ when (meta)sedimentary material is melted) must
170 also be in some way tied to the duration of time between progressive weathering (i.e., increasing
171 $\delta^{18}\text{O}$) and sediment deposition in loci available for incorporation and melting in magmatic
172 systems (e.g., along a subduction trench).

173 **Connecting Land Plants and Zircon**

174 The duration of surface weathering influences the radiogenic ingrowth of Lu-Hf isotopes and
175 mass-dependent fractionation of oxygen isotopes, and is dependent on sediment residence time

176 within the critical zone ⁴⁸. Sediment delivered to rivers at source is then routed through a
177 sediment transfer system. The residence time of a pulse of sediment within this system increases
178 with: 1) the length of the river system; 2) the number of buffers within that system where
179 sediment undergoes transient storage and remains static (e.g., floodplains); and 3) the relative
180 abundance of suspended bed-material load relative to bedload ^{49,50}. The greater sinuosity of
181 meandering channels (compared with braided river networks) means that they are inherently
182 longer routing systems. The associated long-lived floodplains of meandering rivers provide more
183 robust buffers than those in laterally-mobile braided rivers ⁵¹, and sediment transport is more
184 regularly dominated by mixed- or suspended bed-material load. Each of these considerations
185 imply that the time taken for source-to-sink sediment transport is greater in meandering than in
186 braided rivers. Even though individual particles of suspended sediment can be transported more
187 rapidly than bedload within a channel ⁵², individual sediment particles can transit almost five
188 times slower in meandering rivers (9.6 yr km⁻¹) than in braided rivers (1.9 yr km⁻¹) ⁵³. This
189 discrepancy is largely accounted for by residence of particles within hillslope ⁵⁴ and floodplain ⁵⁵
190 staging areas, which are only re-entrained after intervals on the order of 10⁴-10⁵ kyr ^{56,57}, within
191 the timeframe of mature soil development and chemical weathering ^{54,55}.

192 Relevantly, at 430 Myr ago, the empirical shift towards correlated O and Hf-Lu isotopes in
193 zircon is coincident with a global unidirectional shift towards an increased abundance of
194 meandering river channel morphologies (Fig. 3), as tracked by the frequency distribution to
195 physical characteristics of alluvium archived in continental basins ^{10,58}. River sediments
196 deposited after this juncture exhibit a jump in the abundance of mudrock ¹¹ and heterolithic
197 lateral accretion sets ²¹, attesting to a rise in long-lived floodplains, channel stability, and
198 mesoscale sinuosity, that can be mechanistically explained by the novel influence of vegetation
199 acting as a geomorphic agent ^{11,21}. While the specific impact of vegetation manifests at the local

200 scale, the global aggregation of a multitude of local effects (which did not exist prior to c. 430
201 Myr ago) increased the probability of prolonged continental weathering, with downstream
202 impacts on the isotopic composition of the marine sediment ¹³ that could be incorporated into
203 magmatic systems ⁵⁹.

204 Based on the considerable post-430 Myr ago increase of the zircon isotopic correlation (Lu-Hf
205 and $\delta^{18}\text{O}$), we hypothesize a connection between the evolution of land plants and the final fate of
206 sediment in magmatic systems. Following deposition of sedimentary successions along passive
207 margins, these successions were then in prime placement to be subducted along accretionary
208 margins or alternatively get caught in collisional orogens. In both scenarios, sedimentary units
209 are metamorphosed and typically assimilated into arc magmas or melted in collisional systems.
210 The zircon in the resulting magmas exhibit elevated $\delta^{18}\text{O}$ values due to incorporation of
211 sediments. While elevated zircon $\delta^{18}\text{O}$ occurs as early as 4.27 Gyr ago ^{40,41}, critically the
212 coupling between radiogenic isotope systematics (Lu-Hf, U-Pb) and $\delta^{18}\text{O}$ in zircon is absent until
213 after 430 Myr ago.

214 The unidirectional shift in both the zircon and stratigraphic record likely rules out an origin owed
215 to cyclical or episodic geological processes (e.g., tectonic or climatic) as such phenomena have
216 persisted across the planet from the Archean onwards ⁶⁰. The studied interval, from 1200 – 0 Myr
217 ago includes multiple orogenies, numerous alternations between icehouse and greenhouse
218 conditions and the assembly of two supercontinents yet, similar to the unidirectional upsurge in
219 alluvial mudrock ¹¹, none of these extrinsic events appear to have exerted any influence on the
220 observed oxygen and lutetium-hafnium isotopes in zircon. The singular observable shift that
221 does occur, and that we describe, is both coincident with—and explicable by—the onset of more
222 complex vegetation in the late Silurian.

223 We propose that the evolution of land plants led to the stabilization of fluvial systems, resulting
224 in substantial upland weathering and the formation of larger volumes of mud. The resulting
225 higher degrees of weathering along decelerated source-to-sink sediment pathways led to higher
226 $\delta^{18}\text{O}$ signatures in the mud deposited as mudrocks. The eventual melting of this high $\delta^{18}\text{O}$ mud
227 led to higher $\delta^{18}\text{O}$ magmas, providing a direct link between the evolution of the nascent
228 terrestrial biosphere and composition of the lithosphere.

229 **Acknowledgements**

230 This manuscript benefited greatly from discussions with Brenhin Keller. CJS, XW, MS were
231 supported by Natural Sciences and Environment Research Council, Discovery Grant RGPIN-
232 2020-05639. TRM was supported by Natural Sciences and Environment Research Council,
233 Undergraduate Student Research Award 551207 – 2020. TMG and TH were supported by the
234 Turing Institute under the EPSRC grant EP/N510129/1. NSD and WJM were supported by
235 NERC grant NE/T00696X. GML acknowledges support from the State Scholarship Fund of
236 China Scholarship Council (202006410023).

237 **Author contributions:**

238 CJS conceived of the idea and with the help of XW, TRM, MS, NSD, and WJM compiled and
239 interpreted data. CJS, XW, TH, TMG, and GML assisted with the statistical analysis. CJS, XW,
240 WJM, and TH constructed the figures. CJS, NSD, and TMG wrote the manuscript with input
241 from XW, WJM, TRM, TH, PKP, AB, MS, and GML.

242

243 **Competing interests:**

244 Authors declare that they have no competing interests.

246 **Figure Captions**

247 **Fig. 1: ϵHf versus $\delta^{18}\text{O}$ in zircon since 720 Myr ago (A-E).** It is assumed here that all primary
248 magmas are initially derived from the mantle with a $\delta^{18}\text{O}$ of $\sim 5.5\text{‰}$ and a crustal residence time
249 less than ~ 250 Myr (approximating the depleted mantle compositions ⁶¹). The degree of
250 correlation between ϵHf and $\delta^{18}\text{O}_{\text{zircon}}$ is markedly different in the latter two panels (A & B), with
251 the panels covering pre-430 Myr ago showing greater degrees of scatter and weak correlations.
252 F) r^2 versus slope of the regression from 700 Myr ago to 0 Myr ago in 10 Myr steps using a
253 rolling window ⁵.

254 **Fig. 2: Statistical relationship between ϵHf and $\delta^{18}\text{O}$ of zircon.** A step-change algorithm
255 (conjugate partitioned recursion ⁵) demonstrates a statistically valid step change in the slope, r^2
256 and correlation coefficients at either 450 Myr ago (linear regression slope and Pearson's
257 Correlation) or 430 Myr ago (r^2 and Spearman's Rank Correlation). The increase in vascular
258 plants at 450 Myr ago and the increase in mudrock percentage at 430 Myr ago are shown as
259 vertical dashed lines.

260 **Fig. 3: Synthesis of paleontological and sedimentological data from the early Palaeozoic.**
261 Bottom panel: percentage of mudrocks in sedimentary successions from the late Ediacaran
262 through the Carboniferous (data from ref. ¹¹). We find a step change in the abundance of
263 mudrocks at 430 Myr ago ⁵. It is after this point that the correlation between zircon ϵHf and $\delta^{18}\text{O}$
264 increases considerably (Fig. 2). Middle panel: cumulative classification of fluvial rock units
265 through the early Palaeozoic ⁵⁸ showing a shift in the type and diversity of fluvial deposit

266 characteristics at ~430 Myr ago. Top panel: Number of vascular plant species ⁶² and approximate
267 timing of the first land plants, vascular plants, deeper roots, arborescence, and seeds ⁶³.

268 **Fig. 4: Schematic model of fluvial systems both before and after the development of land**
269 **plants.** Prior to the Devonian Period, minimal land plants, rapid channel migration, and river
270 systems dominated by braided rivers led to rapid sediment transfer, minimal development of
271 mud-sized particles, and minor deposition of mudrocks along continental margins. In contrast,
272 after the Devonian, the expansion of vascular land plants led to the development of meandering
273 rivers and the dramatic slowing of sediment transfer to marine environments. These diamic
274 depositional systems influenced the isotopic composition of sediment available for reworking
275 and melting in magmatic systems along destructive plate boundaries.

276
277
278
279
280
281
282
283
284
285
286
287
288
289
290
291
292
293
294
295
296
297

References

1. Bar-On, Y. M., Phillips, R. & Milo, R. The biomass distribution on Earth. *Proceedings of the National Academy of Sciences* **115**, 6506–6511 (2018).
2. Corenblit, D. *et al.* Feedbacks between geomorphology and biota controlling Earth surface processes and landforms: a review of foundation concepts and current understandings. *Earth-Science Reviews* **106**, 307–331 (2011).
3. Brasier, A. T., Culwick, T., Battison, L., Callow, R. H. T. & Brasier, M. D. Evaluating evidence from the Torridonian Supergroup (Scotland, UK) for eukaryotic life on land in the Proterozoic. *Geological Society, London, Special Publications* **448**, 121–144 (2017).
4. Strother, P. K. & Foster, C. A fossil record of land plant origins from charophyte algae. *Science* **373**, 792–796 (2021).
5. Further information is available in the supplementary materials.
6. Rubinstein, C. V, Gerrienne, P., de la Puente, G. S., Astini, R. A. & Steemans, P. Early Middle Ordovician evidence for land plants in Argentina (eastern Gondwana). *New Phytologist* **188**, 365–369 (2010).
7. Wellman, C. H., Steemans, P. & Vecoli, M. Palaeophytogeography of Ordovician–Silurian land plants. *Geological Society, London, Memoirs* **38**, 461–476 (2013).
8. Harrison, C. J. & Morris, J. L. The origin and early evolution of vascular plant shoots and leaves. *Philosophical Transactions of the Royal Society B: Biological Sciences* **373**, 20160496 (2018).
9. Wellman, C. *et al.* Low tropical diversity during the adaptive radiation of early land plants. *Nature Plants* (2021).

- 298 10. Davies, N. S. & Gibling, M. R. Cambrian to Devonian evolution of alluvial systems: The
299 sedimentological impact of the earliest land plants. *Earth-Science Reviews* **98**, 171–200
300 (2010).
- 301 11. McMahon, W. J. & Davies, N. S. Evolution of alluvial mudrock forced by early land plants.
302 *Science* **359**, 1022–1024 (2018).
- 303 12. Rafiei, M. & Kennedy, M. Weathering in a world without terrestrial life recorded in the
304 Mesoproterozoic Velkerri Formation. *Nature communications* **10**, 1–9 (2019).
- 305 13. Kalderon-Asael, B. *et al.* A lithium-isotope perspective on the evolution of carbon and
306 silicon cycles. *Nature* **595**, 394–398 (2021).
- 307 14. Mitchell, R. L. *et al.* Cryptogamic ground covers as analogues for early terrestrial
308 biospheres: Initiation and evolution of biologically mediated proto-soils. *Geobiology* **19**,
309 292–306 (2021).
- 310 15. Hetherington, A. J. & Dolan, L. Stepwise and independent origins of roots among land
311 plants. *Nature* **561**, 235–238 (2018).
- 312 16. Moulton, K. L., West, J. & Berner, R. A. Solute flux and mineral mass balance approaches to
313 the quantification of plant effects on silicate weathering. *American Journal of Science* **300**,
314 539–570 (2000).
- 315 17. Davies, N. S. & McMahon, W. J. Land plant evolution and global erosion rates. *Chemical*
316 *Geology* **567**, 120128 (2021).
- 317 18. Zeichner, S. S. *et al.* Early plant organics increased global terrestrial mud deposition through
318 enhanced flocculation. *Science* **371**, 526–529 (2021).
- 319 19. Berry, C. M. & Fairon-Demaret, M. The architecture of *Pseudosporochnus nodosus* Leclercq
320 et Banks: a Middle Devonian cladoxylopsid from Belgium. *International Journal of Plant*
321 *Sciences* **163**, 699–713 (2002).

- 322 20. Stein, W. E. *et al.* Mid-Devonian Archaeopteris roots signal revolutionary change in earliest
323 fossil forests. *Current biology* **30**, 421–431 (2020).
- 324 21. Davies, N. S. & Gibling, M. R. Paleozoic vegetation and the Siluro-Devonian rise of fluvial
325 lateral accretion sets. *Geology* **38**, 51–54 (2010).
- 326 22. Brasier, A. T. Searching for travertines, calcretes and speleothems in deep time: Processes,
327 appearances, predictions and the impact of plants. *Earth-Science Reviews* **104**, 213–239
328 (2011).
- 329 23. Brasier, A. T., Morris, J. L. & Hillier, R. D. Carbon isotopic evidence for organic matter
330 oxidation in soils of the Old Red Sandstone (Silurian to Devonian, South Wales, UK).
331 *Journal of the Geological Society* **171**, 621–634 (2014).
- 332 24. Moulton, K. L. & Berner, R. A. Quantification of the effect of plants on weathering: Studies
333 in Iceland. *Geology* **26**, 895–898 (1998).
- 334 25. Eiler, J. M. Oxygen isotope variations of basaltic lavas and upper mantle rocks. *Reviews in*
335 *mineralogy and geochemistry* **43**, 319–364 (2001).
- 336 26. McKeegan, K. D. *et al.* The oxygen isotopic composition of the Sun inferred from captured
337 solar wind. *Science* **332**, 1528–1532 (2011).
- 338 27. Clauer, N., O’Neil, J. R. & Bonnot-Courtois, C. The effect of natural weathering on the
339 chemical and isotopic compositions of biotites. *Geochimica et Cosmochimica Acta* **46**,
340 1755–1762 (1982).
- 341 28. Bindeman, I. N., Bekker, A. & Zakharov, D. O. Oxygen isotope perspective on crustal
342 evolution on early Earth: A record of Precambrian shales with emphasis on Paleoproterozoic
343 glaciations and Great Oxygenation Event. *Earth and Planetary Science Letters* **437**, 101–113
344 (2016).

- 345 29. Lipp, A. G. *et al.* The composition and weathering of the continents over geologic time.
346 *Geochemical Perspectives Letters* **7**, 21–26 (2021).
- 347 30. Lenton, T. M., Crouch, M., Johnson, M., Pires, N. & Dolan, L. First plants cooled the
348 Ordovician. *Nature Geoscience* **5**, 86–89 (2012).
- 349 31. Berner, R. A. The rise of plants and their effect on weathering and atmospheric CO₂. *Science*
350 **276**, 544–546 (1997).
- 351 32. Plank, T., Kelley, K. A., Murray, R. W. & Stern, L. Q. Chemical composition of sediments
352 subducting at the Izu-Bonin trench. *Geochemistry, Geophysics, Geosystems* **8**, (2007).
- 353 33. White, W. M. & Dupré, B. Sediment subduction and magma genesis in the Lesser Antilles:
354 isotopic and trace element constraints. *Journal of Geophysical Research: Solid Earth* **91**,
355 5927–5941 (1986).
- 356 34. Spencer, C. J. *et al.* Evidence for melting mud in Earth’s mantle from extreme oxygen
357 isotope signatures in zircon. *Geology* **45**, 975–978 (2017).
- 358 35. Lackey, J. S., Valley, J. W. & Saleeby, J. B. Supracrustal input to magmas in the deep crust
359 of Sierra Nevada batholith: Evidence from high- $\delta^{18}\text{O}$ zircon. *Earth and Planetary Science*
360 *Letters* **235**, 315–330 (2005).
- 361 36. Hopkinson, T. N. *et al.* The identification and significance of pure sediment-derived granites.
362 *Earth and Planetary Science Letters* **467**, 57–63 (2017).
- 363 37. Kemp, A. I. S., Hawkesworth, C. J., Collins, W. J., Gray, C. M. & Blevin, P. L. Isotopic
364 evidence for rapid continental growth in an extensional accretionary orogen: The
365 Tasmanides, eastern Australia. *Earth and Planetary Science Letters* **284**, 455–466 (2009).
- 366 38. Bird, P. An updated digital model of plate boundaries. *Geochemistry, Geophysics,*
367 *Geosystems* **4**, 1–52 (2003).

- 368 39. Valley, J. W. *et al.* 4.4 billion years of crustal maturation: Oxygen isotope ratios of magmatic
369 zircon. *Contributions to Mineralogy and Petrology* **150**, 561–580 (2005).
- 370 40. Cavosie, A. J., Valley, J. W. & Wilde, S. A. Magmatic $\delta^{18}\text{O}$ in 4400-3900 Ma detrital
371 zircons: A record of the alteration and recycling of crust in the Early Archean. *Earth and*
372 *Planetary Science Letters* **235**, 663–681 (2005).
- 373 41. Spencer, C. J. *et al.* Disparities in oxygen isotopes of detrital and igneous zircon identify
374 erosional bias in crustal rock record. *Earth and Planetary Science Letters* **577**, 117248
375 (2022).
- 376 42. Spencer, C. J., Dani, M., Ito, H. & Hoiland, C. Rapid Exhumation of Earth ' s Youngest
377 Exposed Granites Driven by Subduction of an Oceanic Arc Geophysical Research Letters.
378 1–9 (2019) doi:10.1029/2018GL080579.
- 379 43. Bouvier, A., Vervoort, J. D. & Patchett, P. J. The Lu–Hf and Sm–Nd isotopic composition of
380 CHUR: Constraints from unequilibrated chondrites and implications for the bulk
381 composition of terrestrial planets. *Earth and Planetary Science Letters* **273**, 48–57 (2008).
- 382 44. Keller, C. B. *et al.* Neoproterozoic glacial origin of the Great Unconformity. *Proceedings of*
383 *the National Academy of Sciences of the United States of America* **116**, 1136–1145 (2019).
- 384 45. Bucholz, C. E. & Spencer, C. J. Strongly Peraluminous Granites across the Archean-
385 Proterozoic Transition. *Journal of Petrology* **60**, 1299–1348 (2019).
- 386 46. Bindeman, I. N. *et al.* Rapid emergence of subaerial landmasses and onset of a modern
387 hydrologic cycle 2.5 billion years ago. *Nature* **557**, 545–548 (2018).
- 388 47. Liebmann, J. *et al.* Emergence of continents above sea-level influences sediment melt
389 composition. *Terra Nova* (2021) doi:10.1111/ter.12531.
- 390 48. Giardino, J. R. & Houser, C. Introduction to the critical zone. in *Developments in earth*
391 *surface processes* vol. 19 1–13 (Elsevier, 2015).

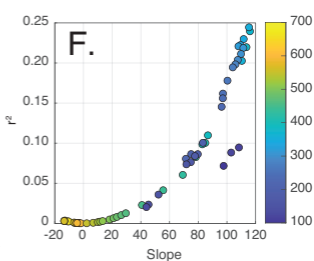
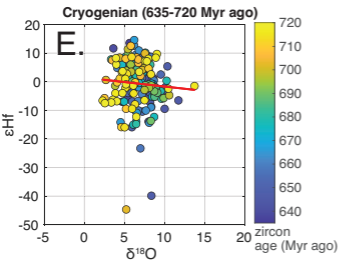
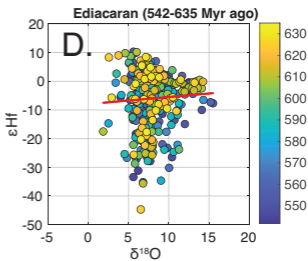
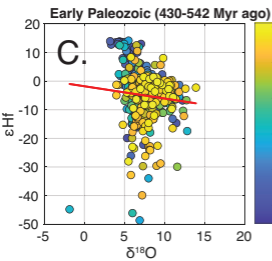
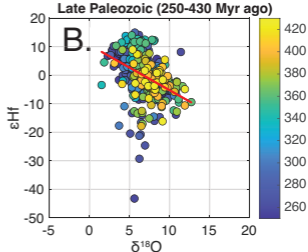
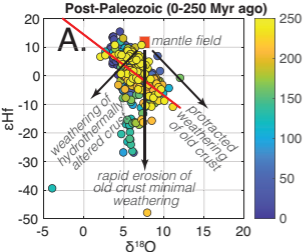
- 392 49. Castelltort, S. & Van Den Driessche, J. How plausible are high-frequency sediment supply-
393 driven cycles in the stratigraphic record? *Sedimentary geology* **157**, 3–13 (2003).
- 394 50. Tofelde, S., Bernhardt, A., Guerit, L. & Romans, B. W. Times associated with source-to-sink
395 propagation of environmental signals during landscape transience. *Frontiers in Earth*
396 *Science* **9**, 227 (2021).
- 397 51. Bufe, A. *et al.* Controls on the lateral channel-migration rate of braided channel systems in
398 coarse non-cohesive sediment. *Earth Surface processes and landforms* **44**, 2823–2836
399 (2019).
- 400 52. Clift, P. D. & Giosan, L. Sediment fluxes and buffering in the post-glacial Indus Basin. *Basin*
401 *Research* **26**, 369–386 (2014).
- 402 53. Repasch, M. *et al.* Sediment transit time and floodplain storage dynamics in alluvial rivers
403 revealed by meteoric ¹⁰Be. *Journal of Geophysical Research: Earth Surface* **125**,
404 e2019JF005419 (2020).
- 405 54. Suresh, P. O., Dosseto, A., Hesse, P. P. & Handley, H. K. Very long hillslope transport
406 timescales determined from uranium-series isotopes in river sediments from a large,
407 tectonically stable catchment. *Geochimica et Cosmochimica Acta* **142**, 442–457 (2014).
- 408 55. Li, C. *et al.* The time scale of river sediment source-to-sink processes in East Asia. *Chemical*
409 *Geology* **446**, 138–146 (2016).
- 410 56. Sheldon, N. D. & Tabor, N. J. Quantitative paleoenvironmental and paleoclimatic
411 reconstruction using paleosols. *Earth-science reviews* **95**, 1–52 (2009).
- 412 57. Ben-Israel, M., Armon, M., Team, A. & Matmon, A. Sediment Residence Times in Large
413 Rivers Quantified Using a Cosmogenic Nuclides Based Transport Model and Implications
414 for Buffering of Continental Erosion Signals. *Journal of Geophysical Research: Earth*
415 *Surface* e2021JF006417.

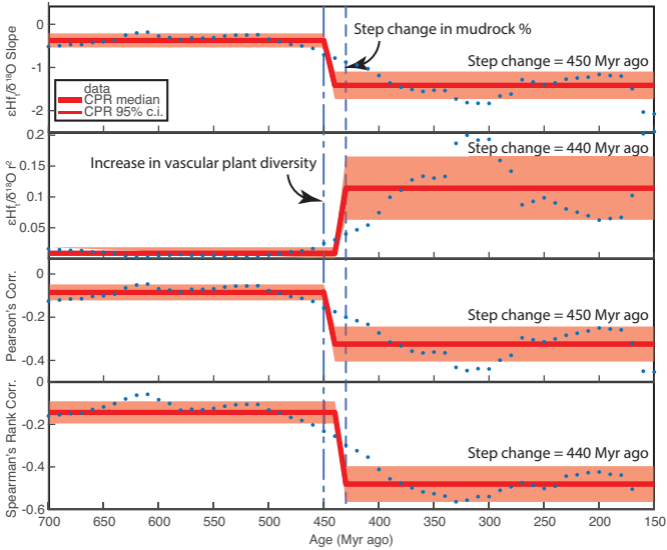
- 416 58. Gibling, M. R. & Davies, N. S. Palaeozoic landscapes shaped by plant evolution. *Nature*
417 *Geoscience* **5**, 99–105 (2012).
- 418 59. Plank, T. & Langmuir, C. H. Tracing trace elements from sediment input to volcanic output
419 at subduction zones. *Nature* **362**, 739–743 (1993).
- 420 60. Davies, N. S. *et al.* Discussion on ‘Tectonic and environmental controls on Palaeozoic fluvial
421 environments: Reassessing the impacts of early land plants on sedimentation’ Journal of the
422 Geological Society, London, <https://doi.org/10.1144/jgs2016-063>. *Journal of the Geological*
423 *Society* **174**, 947–950 (2017).
- 424 61. Jacobsen, S. B. Isotopic constraints on crustal growth and recycling. *Earth and Planetary*
425 *Science Letters* **90**, 315–329 (1988).
- 426 62. Niklas, K. J., Tiffney, B. H. & Knoll, A. H. Patterns in vascular land plant diversification.
427 *Nature* **303**, 614–616 (1983).
- 428 63. Dahl, T. W. & Arens, S. K. M. The impacts of land plant evolution on Earth’s climate and
429 oxygenation state – An interdisciplinary review. *Chemical Geology* **547**, 119665 (2020).
- 430 64. Spencer, C. J., Kirkland, C. L. & Taylor, R. J. M. Strategies towards statistically robust
431 interpretations of in situ U-Pb zircon geochronology. *Geoscience Frontiers* **7**, 581–589
432 (2016).
- 433 65. Spencer, C. J., Kirkland, C. L., Roberts, N. M. W., Evans, N. J. & Liebmann, J. Strategies
434 towards robust interpretations of in situ zircon Lu–Hf isotope analyses. *Geoscience Frontiers*
435 **11**, 843–853 (2020).
- 436 66. Liebmann, J., Spencer, C. J., Kirkland, C. L., Xia, X. P. & Bourdet, J. Effect of water on
437 $\delta^{18}\text{O}$ in zircon. *Chemical Geology* **574**, 120243 (2021).
- 438 67. Spencer, C. J. *et al.* Paleoproterozoic increase in zircon $\delta^{18}\text{O}$ driven by rapid emergence of
439 continental crust. *Geochimica et Cosmochimica Acta* **257**, 16–25 (2019).

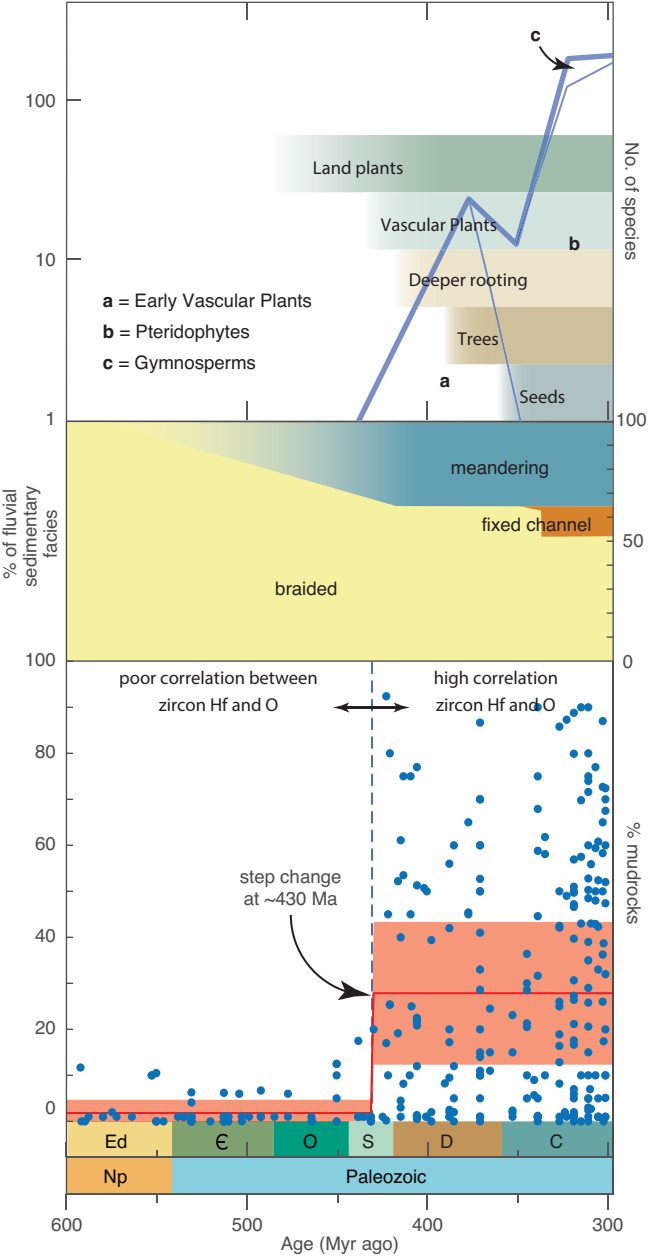
- 440 68. Jensen, G. *Closed-form estimation of multiple change-point models. PeerJ Preprints* (2013)
441 doi:10.7287/peerj.preprints.90v3.
- 442 69. Gallagher, K. *et al.* Inference of abrupt changes in noisy geochemical records using
443 transdimensional changepoint models. *Earth and Planetary Science Letters* **311**, 182–194
444 (2011).
- 445 70. Vervoort, J. D. & Kemp, A. I. S. Clarifying the zircon Hf isotope record of crust-mantle
446 evolution. *Chemical Geology* **425**, 65–75 (2016).
- 447 71. Roberts, N. M. W. & Spencer, C. J. The zircon archive of continent formation through time.
448 in *Geological Society Special Publication* (eds. Roberts, N. M. W., Van Kranendonk, M. J.,
449 Parman, S. W., Shirey, S. B. & Clift, P. D.) vol. 389 197–225 (2015).
- 450 72. Budd, G. E. & Mann, R. P. History is written by the victors: the effect of the push of the past
451 on the fossil record. *Evolution* **72**, 2276–2291 (2018).
- 452 73. Cunningham, J. A., Liu, A. G., Bengtson, S. & Donoghue, P. C. J. The origin of animals: can
453 molecular clocks and the fossil record be reconciled? *BioEssays* **39**, 1–12 (2017).
- 454 74. Dos Reis, M. *et al.* Uncertainty in the timing of origin of animals and the limits of precision
455 in molecular timescales. *Current biology* **25**, 2939–2950 (2015).
- 456 75. Husson, J. M. & Peters, S. E. Nature of the sedimentary rock record and its implications for
457 Earth system evolution. *Emerging Topics in Life Sciences* **2**, 125–136 (2018).
- 458 76. Donoghue, P. C. J., Harrison, C. J., Paps, J. & Schneider, H. The evolutionary emergence of
459 land plants. *Current Biology* **31**, R1281–R1298 (2021).
- 460 77. Roberts, N. M. W. & Spencer, C. J. The zircon archive of continent formation through time.
461 *Geological Society, London, Special Publications* **389**, 197–225 (2015).

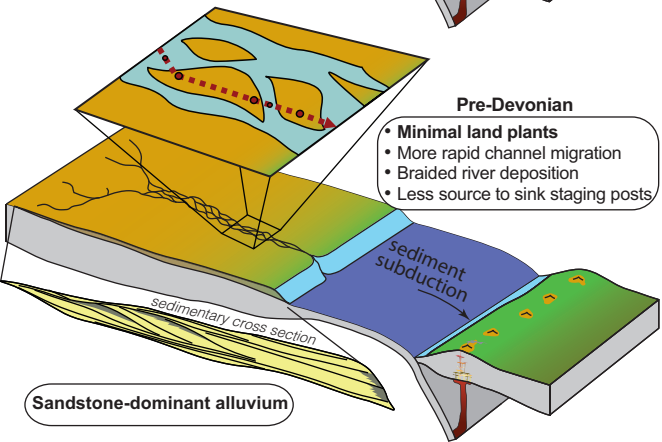
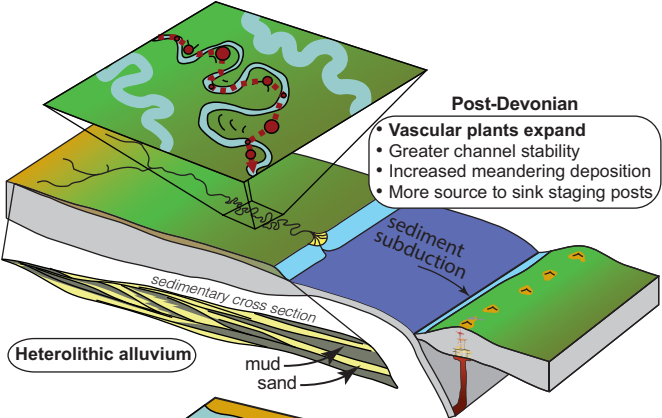
462 78. Spencer, C. *et al.* Disparities in oxygen isotopes of detrital and igneous zircon identify
463 erosional bias in crustal rock record. *Earth and Planetary Science Letters* **577**, 117248
464 (2022).

465 Correspondence and requests for materials should be addressed to CJS.
466









467 **Methods**

468 Data Compilation

469 Data were compiled from 183 publications (Data S1) that included U-Pb, Lu-Hf, and O
470 isotopic analyses of detrital zircon. Only data that passed strict quality control (concordant U-Pb
471 ages ⁶⁴, accurate stable Hf isotope ratios ⁶⁵, and reliable $\delta^{18}\text{O}$ analyses ⁶⁶) were included in our
472 analysis. U-Pb ages, $\epsilon\text{Hf}(t)$, and 2-stage depleted mantle model ages were recalculated using
473 published isotopic ratios using unified decay constants and initial chondritic and depleted mantle
474 values ⁶⁷. Crustal residence times (CR) were calculated by subtracting the U-Pb age from the
475 depleted mantle model age.

476 Statistical Methods

477 We used a rolling window to visualize the change over time in the linear regression slope
478 and R^2 values for CR and $\delta^{18}\text{O}$, and similarly the change in correlation coefficient (Pearson and
479 Spearman's Rank) between CR and $\delta^{18}\text{O}$, and in a separate test, between zircon ϵHf and $\delta^{18}\text{O}$
480 through time (Extended Data Fig. 6).

481 For our purposes, the input time series do not need to be regular; the only requirement is
482 that values for both parameters (CR and $\delta^{18}\text{O}$) exist at any given time step in the time series. We
483 define a window width “w” (e.g., 100 Myr), an increment “i” (e.g., 5 Myr; this is the interval at
484 which we repeat the calculations), and a start and end time.

485 This gives an output timeseries t , from start to end at increments i . At every time step t , we
486 select the data for CR and $\delta^{18}\text{O}$ that lie within the time interval $[t-(w/2), t+(w/2)]$; i.e., a
487 symmetric window centred on t . We then simply calculate the linear regression slope and R^2
488 value for CR and $\delta^{18}\text{O}$ (and separately for zircon ϵHf and $\delta^{18}\text{O}$) using the R function “lm”:

489 $linear_model = lm(CR \sim \delta^{18}O)$

490 The correlation is calculated using the R function, “cor”:

491 $Pearson_correlation = cor(\delta^{18}O, CR)$

492 $Spearman_correlation = cor(\delta^{18}O, CR, method = "spearman")$

493 This process is repeated for all time steps. Note the windows overlap and are centred on the
494 time given on the x axis in the plots shown in figure 2.

495 We next used conjugate partitioned recursion (CPR) to evaluate the potential presence of
496 step changes in the linear regression slope, r^2 and correlation coefficients (Fig. 2). This iterative
497 algorithm uses binary partitioning by marginal likelihood and conjugate priors (conjugate
498 partition recursion) to identify an unknown number of change-points⁶⁸. If the marginal
499 likelihood favours a change-point model, then the algorithm defines a change point and two-
500 sigma uncertainty bounds of the two averages before and after the change point. In applying the
501 CPR algorithm to the correlation statistics data, we identify change-points at 450 Myr ago for
502 ϵHf and $\delta^{18}O$ slope and Pearson’s correlation, and 430 Myr ago for ϵHf and $\delta^{18}O$ r^2 and
503 Spearman’s rank correlation. We also performed CPR to demonstrate the presence of a change-
504 point in the percentage of mudrocks in fluvial sequences using the data of ref.¹¹ (Fig. 3).

505 To further demonstrate the robustness of the change points described above, we also applied
506 a Bayesian change point algorithm using transdimensional Markov chain Monte Carlo⁶⁹. This
507 method infers probability distributions based on the number and locations of changepoints, and
508 the mean values between changepoints. It uses not just a single set of model parameters, but is
509 computed using 10E6 simulations from the probability distribution to evaluate the position of the
510 change points through time using the slope of the regression, r^2 of the regression, Pearson’s
511 correlation, and Spearman’s rank correlation together in its identification of potential change
512 points (Extended Data Fig. 3).

513 *ϵHf versus crustal residence ages*

514 As ϵ_{Hf} is time integrative, comparing ϵ_{Hf} values at different ages result is strictly invalid (e.g.
515 $\epsilon_{\text{Hf}} = 0$ at 200 Ma is not equivalent to $\epsilon_{\text{Hf}} = 0$ at 100 Ma). However, given the narrow windows
516 of time used in this study (<250 Myr), the difference is negligible within our interpretive
517 framework. To address this, we also applied our statistical methods to crustal residence ages
518 compared to $\delta^{18}\text{O}$ through time. Crustal residence time is calculated here as the difference
519 between the U-Pb age and the projected “model age” where the radioactive decay trajectory
520 (controlled by $^{176}\text{Lu}/^{177}\text{Hf}$) intersects with the depleted mantle ⁷⁰. This provides an estimate of
521 how much time elapsed between the initial extraction (or melting) of the mantle and
522 crystallization of zircon. It is important to note that crustal residence times are not geologic ages
523 and are directly tied to depleted mantle model ages. The crustal residence time is generally low
524 when magmas are extracted directly from mantle with zircon forming relatively rapidly, as in
525 subduction zones. In contrast, the crustal residence time is high when ancient crust is remelted
526 100’s of Myrs to ~4 Gyr after initial extraction from the mantle ⁷¹.

527 Timing of plant evolution

528 Here we pinpoint the timing of land plant colonization primarily based on the fossil record.
529 While alternative suggestions of the onset of greening, arising from molecular phylogenies of
530 living plants, suggest an earlier start to the process, there are reasons to be cautious for the
531 statistical biases inherent in these modelling approaches ⁷². A counterargument has been made
532 that molecular phylogenies are closer to the truth for estimating timing because the paucity of
533 non-marine strata in the Cambrian and Ordovician renders its fossil record unreliable; either
534 because that record has been subducted ⁷³ or because there was a limited continental area during
535 the interval ⁷⁴. Both of these arguments are problematic: firstly, because empirically there is no
536 exponential decay of non-marine strata with age, as sometimes envisaged by molecular
537 phylogenists ⁷⁵, and secondly because the abundance of small continents with wide continental

538 shelves during that interval is well suited for preserved fossil evidence for land plants, as the best
539 early record of such comes from dispersed spores preserved in shallow marine strata ⁶. The fossil
540 record thus likely provides a robust estimate of the onset of greening and, regardless, molecular
541 clock analyses and fossil evidence are increasingly convergent on the timing of embryophyte
542 (land plant) origins. Molecular clocks suggest that embryophytes emerged in a mid-Cambrian to
543 Early Ordovician interval ⁷⁶. Recent palynologic evidence favours the end of this bracket and
544 indicates that ancestral embryophytes began evolving from freshwater aquatic charophyte algae
545 around the Early Ordovician (c. 480 Myr ago) ⁴.

546 *Covariance and correlation of Lu-Hf and O isotopes*

547 Keller et al. (2019) reported the covariance between Lu-Hf and O isotopes in zircon. This
548 study used two separate databases that respectively reported Lu-Hf and O isotopes in zircon.
549 They identified a large covariance peak that coincided with the timing of Cryogenian global
550 glaciation and argued in favour of a connection between glaciogenic erosion and the composition
551 of zircon that came from magmas influenced by the assimilation of the resulting flux of
552 glaciogenic sediment into magmatic systems. Their numerical analysis also displayed a second
553 peak of covariance that coincides with the evolution and proliferation of land plants that is the
554 topic of the present study. Although this second Palaeozoic peak in zircon Lu-Hf and O
555 covariance is more prominent in the Keller et al. (2019) study, it was not discussed. Importantly,
556 covariance, as used in the Keller et al. (2019) study, refers to the extent to which two random
557 variables change in tandem. For example, when the slope of secular change in Lu-Hf isotopes
558 and $\delta^{18}\text{O}$ are changing at the same rate then covariance is high. In contrast, correlation measures
559 strength and direction of the linear relationship between two variables. Importantly, it is not
560 possible to measure the strength (or quality) of the linear relationship when using covariance.
561 The Keller et al. study evaluates how Lu-Hf isotopes and $\delta^{18}\text{O}$ change in tandem using

562 independent datasets whereas our study aims to evaluate how strongly Lu-Hf isotopes and $\delta^{18}\text{O}$
563 are directly correlated through time. Interestingly, our study also shows a minor increase in the
564 strength of correlation within the timeframe of the Snowball Earth – however an increase that is
565 a factor of five smaller than the increase in correlation associated with the rise of land plants.

566 Keller et al. (2019) use independent ϵHf and $\delta^{18}\text{O}$ datasets, that is, they use two separate
567 databases for the two isotopic systems. This means their interpretation is limited to a comparison
568 between the secular changes in each dataset and they are unable to directly compare Lu-Hf
569 isotopes and $\delta^{18}\text{O}$ for specific zircon grains. In contrast, our dataset uses only Lu-Hf isotopes and
570 $\delta^{18}\text{O}$ from the same zircon grain providing improved discriminating power in discerning secular
571 changes in the data, which we argue is essential for our purposes. It is assumed each dataset is
572 independently representative, which has previously been demonstrated as not being the case for
573 Lu-Hf isotopes⁷⁷. Further, a later compilation of zircon $\delta^{18}\text{O}$ has shown a significant bias
574 between detrital and igneous zircon⁷⁸ which are indiscriminately combined in Keller et al.
575 (2019). We seek to overcome these issues by comparing Lu-Hf and O isotopes from specific
576 zircon grains.

577 The Keller et al. (2019) study reports two significant peaks in $\delta^{18}\text{O}$ and ϵHf covariance, one
578 at ~650 Ma and the other with higher covariance at ~420 Ma. While they show both peaks in
579 their figure 2, they omit the ~420 Ma peak from their discussion. They posit the ~650 Ma
580 covariance*slope peak is associated with “increasing crustal reworking”, while the large negative
581 covariance*slope trough at ~420 Ma is associated with “decreasing crustal reworking”. N.B. that
582 while they state in the figure caption that a large negative covariance*slope is associated with
583 decreased crustal reworking, they do not state the age of this trough, nor speculate on a potential
584 cause. We posit this ~420 Ma covariance peak is supportive of our hypothesis that the evolution
585 of land plants influenced the covariance of Lu-Hf and O isotopes in zircon.

587
588
589
590
591
592
593
594
595
596
597
598
599
600
601
602
603
604
605
606
607
608

Methods References:

1. Bar-On, Y. M., Phillips, R. & Milo, R. The biomass distribution on Earth. *Proceedings of the National Academy of Sciences* **115**, 6506–6511 (2018).
2. Corenblit, D. *et al.* Feedbacks between geomorphology and biota controlling Earth surface processes and landforms: a review of foundation concepts and current understandings. *Earth-Science Reviews* **106**, 307–331 (2011).
3. Brasier, A. T., Culwick, T., Battison, L., Callow, R. H. T. & Brasier, M. D. Evaluating evidence from the Torridonian Supergroup (Scotland, UK) for eukaryotic life on land in the Proterozoic. *Geological Society, London, Special Publications* **448**, 121–144 (2017).
4. Strother, P. K. & Foster, C. A fossil record of land plant origins from charophyte algae. *Science* **373**, 792–796 (2021).
5. Further information is available in the supplementary materials.
6. Rubinstein, C. V, Gerrienne, P., de la Puente, G. S., Astini, R. A. & Steemans, P. Early Middle Ordovician evidence for land plants in Argentina (eastern Gondwana). *New Phytologist* **188**, 365–369 (2010).
7. Wellman, C. H., Steemans, P. & Vecoli, M. Palaeophytogeography of Ordovician–Silurian land plants. *Geological Society, London, Memoirs* **38**, 461–476 (2013).
8. Harrison, C. J. & Morris, J. L. The origin and early evolution of vascular plant shoots and leaves. *Philosophical Transactions of the Royal Society B: Biological Sciences* **373**, 20160496 (2018).
9. Wellman, C. *et al.* Low tropical diversity during the adaptive radiation of early land plants. *Nature Plants* (2021).

- 609 10. Davies, N. S. & Gibling, M. R. Cambrian to Devonian evolution of alluvial systems: The
610 sedimentological impact of the earliest land plants. *Earth-Science Reviews* **98**, 171–200
611 (2010).
- 612 11. McMahon, W. J. & Davies, N. S. Evolution of alluvial mudrock forced by early land plants.
613 *Science* **359**, 1022–1024 (2018).
- 614 12. Rafiei, M. & Kennedy, M. Weathering in a world without terrestrial life recorded in the
615 Mesoproterozoic Velkerri Formation. *Nature communications* **10**, 1–9 (2019).
- 616 13. Kalderon-Asael, B. *et al.* A lithium-isotope perspective on the evolution of carbon and
617 silicon cycles. *Nature* **595**, 394–398 (2021).
- 618 14. Mitchell, R. L. *et al.* Cryptogamic ground covers as analogues for early terrestrial
619 biospheres: Initiation and evolution of biologically mediated proto-soils. *Geobiology* **19**,
620 292–306 (2021).
- 621 15. Hetherington, A. J. & Dolan, L. Stepwise and independent origins of roots among land
622 plants. *Nature* **561**, 235–238 (2018).
- 623 16. Moulton, K. L., West, J. & Berner, R. A. Solute flux and mineral mass balance approaches to
624 the quantification of plant effects on silicate weathering. *American Journal of Science* **300**,
625 539–570 (2000).
- 626 17. Davies, N. S. & McMahon, W. J. Land plant evolution and global erosion rates. *Chemical*
627 *Geology* **567**, 120128 (2021).
- 628 18. Zeichner, S. S. *et al.* Early plant organics increased global terrestrial mud deposition through
629 enhanced flocculation. *Science* **371**, 526–529 (2021).
- 630 19. Berry, C. M. & Fairon-Demaret, M. The architecture of *Pseudosporochnus nodosus* Leclercq
631 et Banks: a Middle Devonian cladoxylopsid from Belgium. *International Journal of Plant*
632 *Sciences* **163**, 699–713 (2002).

- 633 20. Stein, W. E. *et al.* Mid-Devonian Archaeopteris roots signal revolutionary change in earliest
634 fossil forests. *Current biology* **30**, 421–431 (2020).
- 635 21. Davies, N. S. & Gibling, M. R. Paleozoic vegetation and the Siluro-Devonian rise of fluvial
636 lateral accretion sets. *Geology* **38**, 51–54 (2010).
- 637 22. Brasier, A. T. Searching for travertines, calcretes and speleothems in deep time: Processes,
638 appearances, predictions and the impact of plants. *Earth-Science Reviews* **104**, 213–239
639 (2011).
- 640 23. Brasier, A. T., Morris, J. L. & Hillier, R. D. Carbon isotopic evidence for organic matter
641 oxidation in soils of the Old Red Sandstone (Silurian to Devonian, South Wales, UK).
642 *Journal of the Geological Society* **171**, 621–634 (2014).
- 643 24. Moulton, K. L. & Berner, R. A. Quantification of the effect of plants on weathering: Studies
644 in Iceland. *Geology* **26**, 895–898 (1998).
- 645 25. Eiler, J. M. Oxygen isotope variations of basaltic lavas and upper mantle rocks. *Reviews in*
646 *mineralogy and geochemistry* **43**, 319–364 (2001).
- 647 26. McKeegan, K. D. *et al.* The oxygen isotopic composition of the Sun inferred from captured
648 solar wind. *Science* **332**, 1528–1532 (2011).
- 649 27. Clauer, N., O’Neil, J. R. & Bonnot-Courtois, C. The effect of natural weathering on the
650 chemical and isotopic compositions of biotites. *Geochimica et Cosmochimica Acta* **46**,
651 1755–1762 (1982).
- 652 28. Bindeman, I. N., Bekker, A. & Zakharov, D. O. Oxygen isotope perspective on crustal
653 evolution on early Earth: A record of Precambrian shales with emphasis on Paleoproterozoic
654 glaciations and Great Oxygenation Event. *Earth and Planetary Science Letters* **437**, 101–113
655 (2016).

- 656 29. Lipp, A. G. *et al.* The composition and weathering of the continents over geologic time.
657 *Geochemical Perspectives Letters* **7**, 21–26 (2021).
- 658 30. Lenton, T. M., Crouch, M., Johnson, M., Pires, N. & Dolan, L. First plants cooled the
659 Ordovician. *Nature Geoscience* **5**, 86–89 (2012).
- 660 31. Berner, R. A. The rise of plants and their effect on weathering and atmospheric CO₂. *Science*
661 **276**, 544–546 (1997).
- 662 32. Plank, T., Kelley, K. A., Murray, R. W. & Stern, L. Q. Chemical composition of sediments
663 subducting at the Izu-Bonin trench. *Geochemistry, Geophysics, Geosystems* **8**, (2007).
- 664 33. White, W. M. & Dupré, B. Sediment subduction and magma genesis in the Lesser Antilles:
665 isotopic and trace element constraints. *Journal of Geophysical Research: Solid Earth* **91**,
666 5927–5941 (1986).
- 667 34. Spencer, C. J. *et al.* Evidence for melting mud in Earth’s mantle from extreme oxygen
668 isotope signatures in zircon. *Geology* **45**, 975–978 (2017).
- 669 35. Lackey, J. S., Valley, J. W. & Saleeby, J. B. Supracrustal input to magmas in the deep crust
670 of Sierra Nevada batholith: Evidence from high- $\delta^{18}\text{O}$ zircon. *Earth and Planetary Science*
671 *Letters* **235**, 315–330 (2005).
- 672 36. Hopkinson, T. N. *et al.* The identification and significance of pure sediment-derived granites.
673 *Earth and Planetary Science Letters* **467**, 57–63 (2017).
- 674 37. Kemp, A. I. S., Hawkesworth, C. J., Collins, W. J., Gray, C. M. & Blevin, P. L. Isotopic
675 evidence for rapid continental growth in an extensional accretionary orogen: The
676 Tasmanides, eastern Australia. *Earth and Planetary Science Letters* **284**, 455–466 (2009).
- 677 38. Bird, P. An updated digital model of plate boundaries. *Geochemistry, Geophysics,*
678 *Geosystems* **4**, 1–52 (2003).

- 679 39. Valley, J. W. *et al.* 4.4 billion years of crustal maturation: Oxygen isotope ratios of magmatic
680 zircon. *Contributions to Mineralogy and Petrology* **150**, 561–580 (2005).
- 681 40. Cavosie, A. J., Valley, J. W. & Wilde, S. A. Magmatic $\delta^{18}\text{O}$ in 4400-3900 Ma detrital
682 zircons: A record of the alteration and recycling of crust in the Early Archean. *Earth and*
683 *Planetary Science Letters* **235**, 663–681 (2005).
- 684 41. Spencer, C. J. *et al.* Disparities in oxygen isotopes of detrital and igneous zircon identify
685 erosional bias in crustal rock record. *Earth and Planetary Science Letters* **577**, 117248
686 (2022).
- 687 42. Spencer, C. J., Dani, M., Ito, H. & Hoiland, C. Rapid Exhumation of Earth ' s Youngest
688 Exposed Granites Driven by Subduction of an Oceanic Arc Geophysical Research Letters.
689 1–9 (2019) doi:10.1029/2018GL080579.
- 690 43. Bouvier, A., Vervoort, J. D. & Patchett, P. J. The Lu–Hf and Sm–Nd isotopic composition of
691 CHUR: Constraints from unequilibrated chondrites and implications for the bulk
692 composition of terrestrial planets. *Earth and Planetary Science Letters* **273**, 48–57 (2008).
- 693 44. Keller, C. B. *et al.* Neoproterozoic glacial origin of the Great Unconformity. *Proceedings of*
694 *the National Academy of Sciences of the United States of America* **116**, 1136–1145 (2019).
- 695 45. Bucholz, C. E. & Spencer, C. J. Strongly Peraluminous Granites across the Archean-
696 Proterozoic Transition. *Journal of Petrology* **60**, 1299–1348 (2019).
- 697 46. Bindeman, I. N. *et al.* Rapid emergence of subaerial landmasses and onset of a modern
698 hydrologic cycle 2.5 billion years ago. *Nature* **557**, 545–548 (2018).
- 699 47. Liebmann, J. *et al.* Emergence of continents above sea-level influences sediment melt
700 composition. *Terra Nova* (2021) doi:10.1111/ter.12531.
- 701 48. Giardino, J. R. & Houser, C. Introduction to the critical zone. in *Developments in earth*
702 *surface processes* vol. 19 1–13 (Elsevier, 2015).

- 703 49. Castelltort, S. & Van Den Driessche, J. How plausible are high-frequency sediment supply-
704 driven cycles in the stratigraphic record? *Sedimentary geology* **157**, 3–13 (2003).
- 705 50. Tofelde, S., Bernhardt, A., Guerit, L. & Romans, B. W. Times associated with source-to-sink
706 propagation of environmental signals during landscape transience. *Frontiers in Earth
707 Science* **9**, 227 (2021).
- 708 51. Bufe, A. *et al.* Controls on the lateral channel-migration rate of braided channel systems in
709 coarse non-cohesive sediment. *Earth Surface processes and landforms* **44**, 2823–2836
710 (2019).
- 711 52. Clift, P. D. & Giosan, L. Sediment fluxes and buffering in the post-glacial Indus Basin. *Basin
712 Research* **26**, 369–386 (2014).
- 713 53. Repasch, M. *et al.* Sediment transit time and floodplain storage dynamics in alluvial rivers
714 revealed by meteoric ¹⁰Be. *Journal of Geophysical Research: Earth Surface* **125**,
715 e2019JF005419 (2020).
- 716 54. Suresh, P. O., Dosseto, A., Hesse, P. P. & Handley, H. K. Very long hillslope transport
717 timescales determined from uranium-series isotopes in river sediments from a large,
718 tectonically stable catchment. *Geochimica et Cosmochimica Acta* **142**, 442–457 (2014).
- 719 55. Li, C. *et al.* The time scale of river sediment source-to-sink processes in East Asia. *Chemical
720 Geology* **446**, 138–146 (2016).
- 721 56. Sheldon, N. D. & Tabor, N. J. Quantitative paleoenvironmental and paleoclimatic
722 reconstruction using paleosols. *Earth-science reviews* **95**, 1–52 (2009).
- 723 57. Ben-Israel, M., Armon, M., Team, A. & Matmon, A. Sediment Residence Times in Large
724 Rivers Quantified Using a Cosmogenic Nuclides Based Transport Model and Implications
725 for Buffering of Continental Erosion Signals. *Journal of Geophysical Research: Earth
726 Surface* e2021JF006417.

- 727 58. Gibling, M. R. & Davies, N. S. Palaeozoic landscapes shaped by plant evolution. *Nature*
728 *Geoscience* **5**, 99–105 (2012).
- 729 59. Plank, T. & Langmuir, C. H. Tracing trace elements from sediment input to volcanic output
730 at subduction zones. *Nature* **362**, 739–743 (1993).
- 731 60. Davies, N. S. *et al.* Discussion on ‘Tectonic and environmental controls on Palaeozoic fluvial
732 environments: Reassessing the impacts of early land plants on sedimentation’ Journal of the
733 Geological Society, London, <https://doi.org/10.1144/jgs2016-063>. *Journal of the Geological*
734 *Society* **174**, 947–950 (2017).
- 735 61. Jacobsen, S. B. Isotopic constraints on crustal growth and recycling. *Earth and Planetary*
736 *Science Letters* **90**, 315–329 (1988).
- 737 62. Niklas, K. J., Tiffney, B. H. & Knoll, A. H. Patterns in vascular land plant diversification.
738 *Nature* **303**, 614–616 (1983).
- 739 63. Dahl, T. W. & Arens, S. K. M. The impacts of land plant evolution on Earth’s climate and
740 oxygenation state – An interdisciplinary review. *Chemical Geology* **547**, 119665 (2020).
- 741 64. Spencer, C. J., Kirkland, C. L. & Taylor, R. J. M. Strategies towards statistically robust
742 interpretations of in situ U-Pb zircon geochronology. *Geoscience Frontiers* **7**, 581–589
743 (2016).
- 744 65. Spencer, C. J., Kirkland, C. L., Roberts, N. M. W., Evans, N. J. & Liebmann, J. Strategies
745 towards robust interpretations of in situ zircon Lu–Hf isotope analyses. *Geoscience Frontiers*
746 **11**, 843–853 (2020).
- 747 66. Liebmann, J., Spencer, C. J., Kirkland, C. L., Xia, X. P. & Bourdet, J. Effect of water on
748 $\delta^{18}\text{O}$ in zircon. *Chemical Geology* **574**, 120243 (2021).
- 749 67. Spencer, C. J. *et al.* Paleoproterozoic increase in zircon $\delta^{18}\text{O}$ driven by rapid emergence of
750 continental crust. *Geochimica et Cosmochimica Acta* **257**, 16–25 (2019).

- 751 68. Jensen, G. *Closed-form estimation of multiple change-point models. PeerJ Preprints* (2013)
752 doi:10.7287/peerj.preprints.90v3.
- 753 69. Gallagher, K. *et al.* Inference of abrupt changes in noisy geochemical records using
754 transdimensional changepoint models. *Earth and Planetary Science Letters* **311**, 182–194
755 (2011).
- 756 70. Vervoort, J. D. & Kemp, A. I. S. Clarifying the zircon Hf isotope record of crust-mantle
757 evolution. *Chemical Geology* **425**, 65–75 (2016).
- 758 71. Roberts, N. M. W. & Spencer, C. J. The zircon archive of continent formation through time.
759 in *Geological Society Special Publication* (eds. Roberts, N. M. W., Van Kranendonk, M. J.,
760 Parman, S. W., Shirey, S. B. & Clift, P. D.) vol. 389 197–225 (2015).
- 761 72. Budd, G. E. & Mann, R. P. History is written by the victors: the effect of the push of the past
762 on the fossil record. *Evolution* **72**, 2276–2291 (2018).
- 763 73. Cunningham, J. A., Liu, A. G., Bengtson, S. & Donoghue, P. C. J. The origin of animals: can
764 molecular clocks and the fossil record be reconciled? *BioEssays* **39**, 1–12 (2017).
- 765 74. Dos Reis, M. *et al.* Uncertainty in the timing of origin of animals and the limits of precision
766 in molecular timescales. *Current biology* **25**, 2939–2950 (2015).
- 767 75. Husson, J. M. & Peters, S. E. Nature of the sedimentary rock record and its implications for
768 Earth system evolution. *Emerging Topics in Life Sciences* **2**, 125–136 (2018).
- 769 76. Donoghue, P. C. J., Harrison, C. J., Paps, J. & Schneider, H. The evolutionary emergence of
770 land plants. *Current Biology* **31**, R1281–R1298 (2021).
- 771 77. Roberts, N. M. W. & Spencer, C. J. The zircon archive of continent formation through time.
772 *Geological Society, London, Special Publications* **389**, 197–225 (2015).

773 78. Spencer, C. *et al.* Disparities in oxygen isotopes of detrital and igneous zircon identify
774 erosional bias in crustal rock record. *Earth and Planetary Science Letters* **577**, 117248
775 (2022).
776

Composition of continental crust altered by the emergence of land plants

Christopher J. Spencer^{1*}, Neil S. Davies², Thomas M. Gernon³, Xi Wang¹, William J. McMahon², Taylor Rae Morrell¹, Thea Hincks³, Peir K. Pufahl¹, Alexander Brasier⁴, Marina Seraine¹, Gui-Mei Lu^{1,5}

*Corresponding author. Email: c.spencer@queensu.ca

¹Department of Geological Sciences and Geological Engineering, Queen's University; Kingston K7L 2N8, Ontario, Canada

²Department of Earth Sciences, University of Cambridge; Downing Street, Cambridge CB2 3EQ, United Kingdom

³School of Ocean & Earth Science, University of Southampton; Southampton SO14 3ZH, United Kingdom

⁴School of Geosciences, University of Aberdeen, King's College; Aberdeen AB24 3UE, United Kingdom

⁵State Key Laboratory of Geological Processes and Mineral Resources, School of Earth Sciences, China University of Geosciences; Wuhan 430074, China

Extended Data Figures and Tables

This PDF includes:

Extended Data Figures 1-6

Extended Data Table 1

Extended Data Figure Captions

Extended Data Fig. 1: Secular plot of $\delta^{18}\text{O}$ in mudrocks and zircon during different Periods in the Palaeozoic. Note that no systematic or long-term change in shale composition is present throughout the Phanerozoic. Mudrock $\delta^{18}\text{O}$ data are from ^{34,79,80}. Uncertainty bars are 2 S.D.

Extended Data Fig. 2: Transdimensional Markov chain Monte Carlo simulation of the zircon crustal residence versus $\delta^{18}\text{O}$ slope, r^2 , and correlation coefficients demonstrates a statistically valid change point between 450-410 Myr ago with a maximum likelihood at 440 Myr ago (using one million simulations).

31 **Extended Data Fig. 3: Transdimensional Markov chain Monte Carlo (MCMC) simulation**
32 **and conjugate partitioned recursion (CPR) of the percentage of mudrocks through time.**
33 Data from ref. ¹⁷. MCMC yields a statistically valid change point between 430-420 Myr ago with
34 a maximum likelihood at 423 Myr ago (using one million simulations) whereas CPR shows a
35 change point at 430 Myr ago.

36 **Extended Data Fig. 4: Crustal residence time vs $\delta^{18}\text{O}$ in zircon through time.** This includes
37 (A) the Archean Eon (pre-2500 Myr ago), and major supercontinent assembly events including
38 (B) Nuna from 2200 to 1700 Myr ago, (C) Columbia from 1700 to 1200 Myr ago, (D) Rodinia
39 from 1200-900 Myr ago, Pangea from 400-250 Myr ago, and (F) post-Pangea assembly from 250
40 Myr ago to present.

41
42 **Extended Data Fig. 5: Crustal residence versus $\delta^{18}\text{O}$ in zircon since 720 Myr ago (A-E).** It
43 is assumed here that all primary magmas are initially derived from the mantle with a $\delta^{18}\text{O}$ of
44 $\sim 5.5\%$ and a crustal residence time less than ~ 250 Myr (approximating the depleted mantle
45 compositions ⁶¹). The degree of correlation between ϵHf and $\delta^{18}\text{O}_{\text{zircon}}$ is markedly different in
46 the latter two panels (A & B), with the panels covering pre-430 Myr ago showing greater degrees
47 of scatter and weak correlations. F) r^2 versus slope of the regression from 700 Myr ago to 0 Myr
48 ago in 10 Myr steps using a rolling window.

49
50 **Extended Data Fig. 6: Statistical relationship between zircon ϵHf and $\delta^{18}\text{O}$ through time.** A
51 step-change algorithm (conjugate partitioned recursion ⁵) demonstrates a statistically valid step
52 change in the slope, r^2 and correlation coefficients at either 450 Myr ago (linear regression slope
53 and Pearson's Correlation) or 430 Myr ago (r^2 and Spearman's Rank Correlation). The increase
54 in vascular plants at 450 Myr ago and the increase in mudrock percentage at 430 Myr ago are
55 shown as vertical dashed lines.

56
57 **Extended Data Table 1. (Separate file)**

58
59 Compiled zircon U-Pb, Lu-Hf, and $\delta^{18}\text{O}$ database.

